Available online at www.sciencedirect.com
SCIENCE DIRECT®
PERGAMON
International Journal of Heat and Mass Transfer 46 (2003) 2785–2797
International Journal of HEAT and MASS TRANSFER
www.elsevier.com/locate/ijhmt

Constructal tree-shaped two-phase flow for cooling a surface

C. Zamfirescu, A. Bejan *

Department of Mechanical Engineering and Materials Science, Duke University, P.O. Box 90300, Durham, NC 27708-0300, USA

Received 11 October 2002; received in revised form 9 January 2003

Abstract

This paper documents the strong relation that exists between the changing architecture of a complex flow system and the maximization of global performance under constraints. The system is a surface with uniform heating per unit area, which is cooled by a network with evaporating two-phase flow. Illustrations are based on the design of the cooling network for a skating rink. The flow structure is optimized as a sequence of building blocks, which starts with the smallest (elemental volume of fixed size), and continues with assemblies of stepwise larger sizes (first construct, second construct, etc.). The optimized flow network is tree shaped. Three features of the elemental volume are optimized: the cross-sectional shape, the elemental tube diameter, and the shape of the elemental area viewed from above. The tree that emerges at larger scales is optimized for minimal amount of header material and fixed pressure drop. The optimal number of constituents in each new (larger) construct decreases as the size and complexity of the construct increase. Constructs of various levels of complexity compete: the paper shows how to select the optimal flow structure subject to fixed size (cooled surface), pressure drop and amount of header material.

Keywords: Constructal theory; Two-phase flow; Tree networks; Constructal design; Dendritic; Hierarchical structures; Topology optimization; Heat exchangers; Skating rinks

1. Introduction

Constructal theory [1] is a hierarchical way of thinking that accounts for organization, complexity and diversity in nature, engineering and management. It was first stated in 1996 in the context of optimizing the access to flow between a point and an area, with application to traffic and the cooling of electronics: "For a finite-size open system to persist in time (to survive) it must evolve in such a way that it provides easier and easier access to the currents that flow through it." The flow path was constructed in a sequence of steps that starts with the smallest building block (elemental area) and continued in time with larger building blocks (assemblies or constructs). The mode of transport with the highest resistivity (slow flow, diffusions, walking, and high cost) was placed at the smallest scales, filling completely the smallest elements. Modes of transport with successively lower resistivities (fast flow, streams, vehicles, and low cost) were placed in the larger constructs, where they were used to connect the area-point or volume-point flows integrated over the constituents. The geometry of each building block was optimized for area-point access. The constructal architecture that emerged was a tree in which every geometric detail is a result—the tree, as a geometric form *deduced* from a principle.

The thought that the same objective and constraints principle anticipates the occurrence of flow structure in natural system was named *constructal theory*. The application of the principle in the development of engineered flow architectures is *constructal design*. For example, it was shown [1–3] that a volume that generates heat at every point can be cooled with one stream by distributing the stream through the volume as a tree-shaped network, and by recollecting the stream by using a second tree. The canopies of the two trees were superimposed, so that every heat-generating point of the volume was served by an arriving mini-stream of coolant, and by a departing mini-stream of heated fluid. In

* Corresponding author. Tel.: +1-919-660-5309; fax: +1-919-660-8963.
E-mail address: dalford@duke.edu (A. Bejan).

0017-9310/03/$ - see front matter
doi:10.1016/S0017-9310(03)00043-7

Nomenclature

a	diameter ratio defined by Eqs. (32) and (55)
A	area, m^2
A	relative amount of materials for headers, Eqs. (43), (56) and (57)
C	coefficient, Eq. (37)
c_1	factor, Eq. (26), $m^{-3.75}$
D	diameter, m
f	friction coefficient for distributed pressure drop
F	two-phase multiplier for convective component of heat transfer coefficient
h	heat transfer coefficient, $W/m^2\,K$
H	height, m
Δh	latent heat of vaporization, J/kg
k	thermal conductivity, W/mK, or index
m	exponent, Eq. (7)
M	molecular mass, kg/kmol
$\dot{m}$	mass flow rate, kg/s
n	index, exponent or recirculation ratio
p	pressure, Pa
Pr	Prandtl number
$\dot{Q}$	thermal power, W
q''	heat flux, W/m^2
R_a	roughness, m
R_{a0}	reference roughness, 10^{-6} m
Re	Reynolds number
S	suppression factor for nucleate component of heat transfer coefficient
T	temperature, K
U	liquid velocity, m/s
v	specific volume, m^3/kg
W	width, m
x	coordinate, m
x	vapor quality
X	Lockhart–Martinelli parameter
y	coordinate, m

Greek symbols

η	dynamic viscosity, Pa s
θ	dimensionless temperature difference
ν	kinematic viscosity, m^2/s
ξ	longitudinal coordinate, m
ρ	density, kg/m^3
Φ	two-phase flow multiplier for distributed pressure drop
ψ	two-phase flow multiplier for local pressure drop

Subscripts

0	elemental volume
1	inlet, horizontal plane, first construct
2	outlet
ab	between port "a" and "b"
ac	between port "a" and "c"
b	nucleate boiling component or boiling fluid
c	convective component or collecting header
cd	between point "c" and "d"
cr	critical pressure
d	distributing header
dc	between point "d" and "c"
i, j, k	indexes
L	liquid, linear
LO	liquid only
LV	vapor–liquid
M	molecular mass effect
NB	nucleate boiling
opt	optimal
out	outlet
p	pressure effect
peak	peak temperature
r	reduced pressure, $p_r = p/p_{cr}$
tt	turbulent vapor and liquid
TP	two-phase
V	vapor
VO	vapor only
w	wall
x	vapor quality effect

terms of the tree analogs of river flow, the constructal design consisted of designing over the given volume a delta (the arriving coolant) superimposed over a river drainage basin (the departing tree of heated fluid). At each point in the volume, the fluid flowed from the delta into the drainage basin, while removing the heat that was generated locally.

Similar superpositions of tree canopies rule the design of many flow structures in living systems. Circulatory systems and vascularized tissues are configured as two trees matched canopy to canopy. Arterial blood arrives through a capillary vessel at the smallest (elemental) volume of the vascularized tissue, and, later, the same mini-stream departs as venous blood toward the heart. Lungs are time-dependent (two-stroke) analogs of the same two-tree design. The elemental volume (alveolus) receives a puff of oxygenated air during inhalation, and returns the same puff as CO_2-rich air during exhalation. The O_2 and CO_2 air flow trees are superimposed, and their smallest ramifications are connected in each elemental volume. This is why the matched trees are the most effective flow structure: every single elemental volume is served by fluid that, by necessity, must enter and exit the large volume as one large stream.

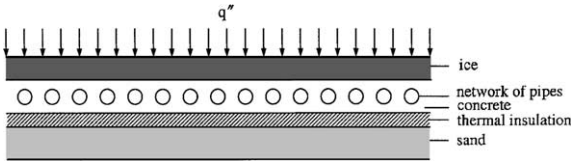

Fig. 1. The multilayer structure of the ice floor of a skating rink.

In the matched-tree design of Refs. [1–3] the fluid was single phase. In this paper we consider the more complex and potentially more important application of this design approach to volumes cooled by streams that undergo evaporation. The change of phase is attractive from the point of view of increasing the cooling rate per unit volume. On the other hand, the presence of phase change complicates the design because of inherently non-smooth distributions of temperature and pressure along each elemental duct. Fundamentally, the same issues are relevant to the design of volumes that must be heated at every point by a tree of condensing fluid.

There are many applications in which phase-change cooling must be distributed over entire areas and volumes. The ice of a skating rink is maintained by the cooling effect provided by a stream of evaporating refrigerant. The heating comes from the atmosphere. The volume discussed in the preceding paragraphs is two-dimensional (flat), and the volumetric heating rate is the heat flux (q'') that arrives at the exposed surface of the ice layer. A vertical cut through the ice floor is illustrated in Fig. 1. A good assumption is that the heat flux q'' is constant, and that the layers placed under the floor insulate perfectly the underside of the structure. According to this model, the volume inhabited by the floor structure is a volume with uniformly distributed heat generation. The purpose of the piping network is to provide volumetric cooling in the most uniform manner possible, and with minimal pumping power.

Similar applications of this geometric optimization of two-phase flow distribution are found in the cooling of electronics, where the two-dimensional volume is heated by electronic circuits, components, and modules [1,4]. Additional examples are in air conditioning: the cooling of an entire ceiling [5], the heat-pump heat exchanger between the ground and the fluid loop (water, air) [6], heat pumps driven by solar heating, where the solar panel contains a distributed desorber [7], and various cold storage applications [8].

2. Constructal tree flow structure

According to the constructal method, we view the given volume as a morphing flow structure, which is a construction made of building blocks of increasing sizes.

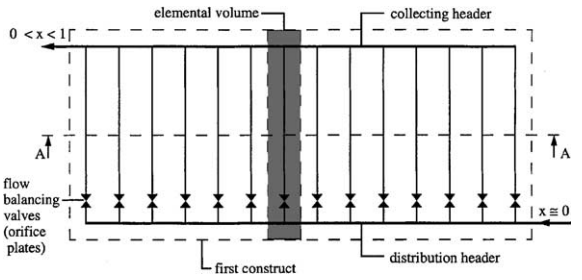

Fig. 2. First construct consisting of a number of elemental volumes.

The volume is flat (two-dimensional) as in the example shown in Fig. 2. It is bathed by one stream ($\dot{m}$), and the heat addition per unit area is uniform (q''). In the sample of Fig. 2, the volume is a *first construct*, i.e. an assembly of a number of *elemental volumes*. Each elemental volume is cooled by a single pipe, which houses the smallest stream of the ensuing flow network. The elemental volume is the smallest volume scale of the flow structure that will eventually fill the given volume. Fig. 3 shows a transversal cut (section A–A) through the elemental volumes of Fig. 2.

The first construct chosen for illustration in Fig. 2 shows already how two tree flow structures are being matched canopy to canopy. If the plane A–A cuts through the middle of each elemental volume, then the flow structure situated below this plane is the tree that distributes the fluid, while the upper structure is the tree that reconstitutes the stream. In this first-construct example, each tree is a comb, or a rake. The top and bottom headers are the stems. The single inlet and the single outlet are the roots (source, sink) of the two trees.

Fig. 4 shows the design direction that can be followed in order to cover larger volumes with increasingly more complex tree flow structures. The second construct indicated in Fig. 4 is made of three first constructs of the type shown in Fig. 2. The entire structure of Fig. 4 is a third construct, which consists of two second constructs. The analysis described next outlines the application of the objective and constraints principle in pursuit of the optimal geometric features of the flow structure. The strategy is to minimize the resistance to heat and fluid flow at every step.

3. Optimal elemental cross-section

We begin with the optimization of the cross-sectional shape of each elemental volume. This is an important and very basic heat conduction optimization opportunity, because at this smallest volume scale the heat q'' must flow by thermal diffusion through solid (e.g.,

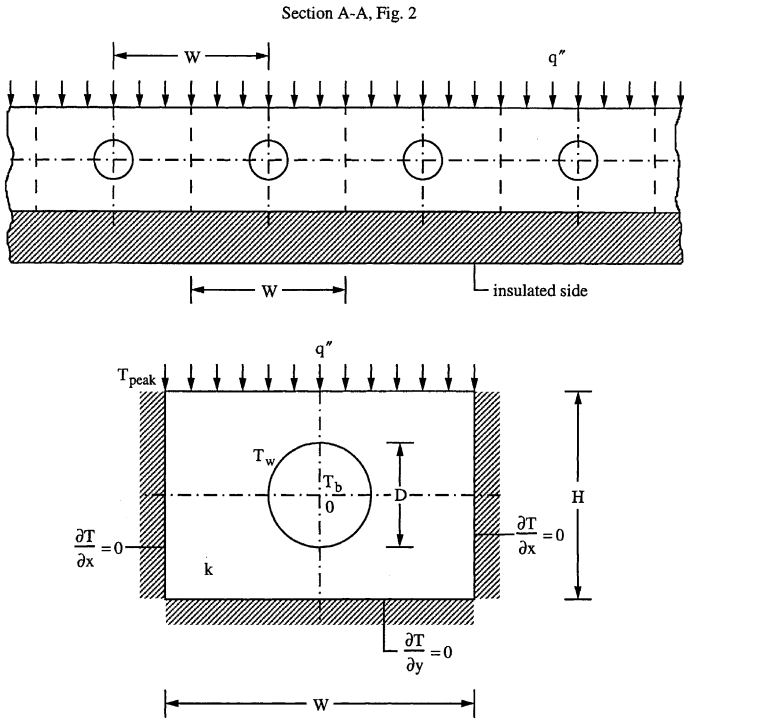

Fig. 3. Transversal cut through the elemental volumes shown in Fig. 2.

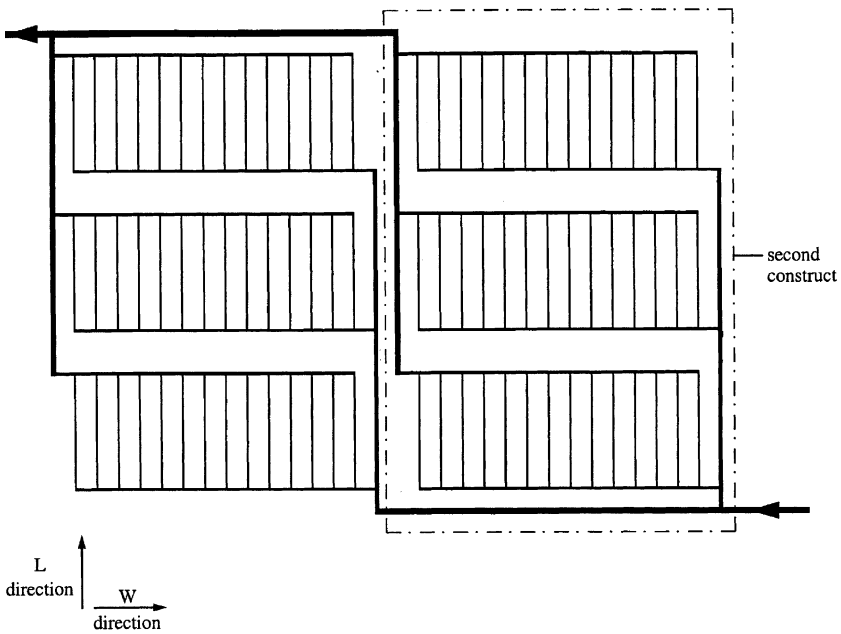

Fig. 4. Larger volumes can be cooled with increasingly complex flow structures: a third construct consisting of two second constructs. Each second construct is an assembly of three first constructs.

concrete) before reaching the cooling surface of the embedded pipe (T_w). The solid conduction domain of thermal conductivity k is shown in the lower part of Fig. 3. The size of the domain is fixed,

$$A = HW, \quad \text{constant} \tag{1}$$

The thermal boundary conditions are indicated on the figure. The temperature field $T(x, y)$ in the 'rectangle with hole' domain is obtained by solving the steady state energy equation

$$\frac{\partial^2 T}{\partial x^2} + \frac{\partial^2 T}{\partial y^2} = 0 \tag{2}$$

We performed these computations by solving the conduction problem in dimensionless form, by using a finite element method [9]. The highest temperatures occur in the vicinity of the upper boundary, which receives q''. The peak temperature (T_{peak}) occurs in the two upper corners. In the skating rink example of Fig. 1, the allowable peak temperature is lower than the melting point of ice. The temperature along the line between the two T_{peak} corners is lower than T_{peak}. A good design is the one in which the surface temperature is nearly uniform, again, subject to real life constraints such as Eq. (1). The search for this configuration is the same as the minimization of the global temperature difference across the entire A domain, namely $T_{\text{peak}} - T_{\text{w}}$. The configuration has two degrees of freedom, which are represented by the shape H/W and the ratio $D/A^{1/2}$. The latter represents the volume allocated to duct flow relative to the total volume (duct space and solid).

Fig. 5 shows one optimized cross-sectional geometry. When $D/A^{1/2} = 0.565$, the optimal aspect ratio of the domain is $(H/W)_{\text{opt}} = 0.83$. This ratio does not depend on k and q''. It depends only on the assumed value of $D/A^{1/2}$. By performing H/W optimizations for other $D/A^{1/2}$ values we constructed Fig. 6, which shows that $(H/W)_{\text{opt}}$ is relatively insensitive to changes in $D/A^{1/2}$.

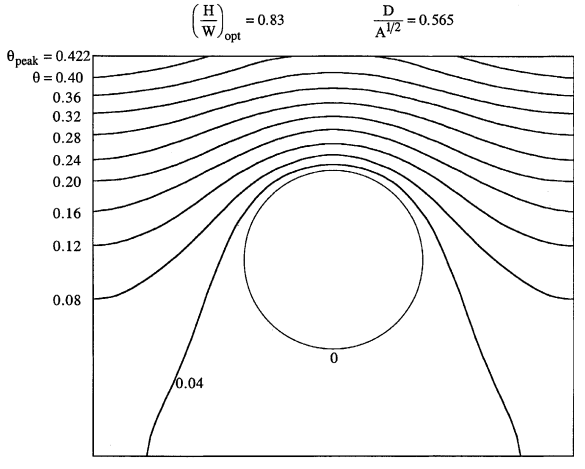

Fig. 5. Temperature distribution in one optimized elemental cross-section.

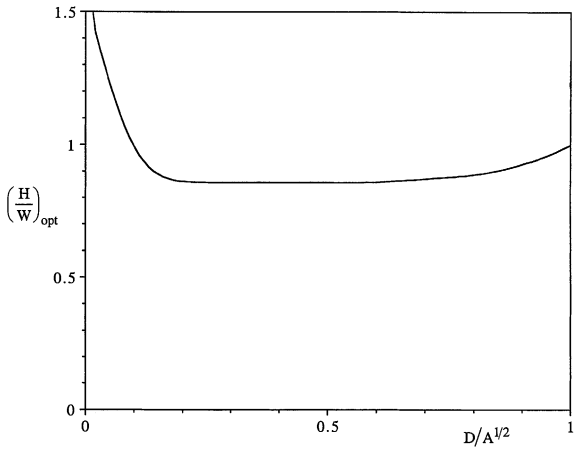

Fig. 6. The effect of the tube size on the optimized aspect ratio of the elemental cross-section.

The two extremes of the $D/A^{1/2}$ range are not practical. When $D/A^{1/2} < 0.1$ the overall thermal resistance (θ_{peak}) is too large, while in the range $0.8 < D/A^{1/2} < 1$ the large D weakens the mechanical structure. This means that the example of Fig. 5 illustrates the optimal H/W ratio for a wide range of intermediate and practical $D/A^{1/2}$ values.

4. Optimal tube diameter

Next, we search for the optimal tube wall temperature (T_{w}) by minimizing the overall temperature difference between the two-phase flow (saturation temperature T_{b}) and the highest temperature in the elemental cross-section (T_{peak}). The optimal T_{w} value results from the competition between conductances on the solid side (k) and fluid side (hD).

The heat transfer coefficient (h) is commonly estimated by modeling forced convection boiling as a superposition of two heat transfer mechanisms, forced convection and (h_{c}) nucleate boiling (h_{b}) [10–13]. Forced convection is the dominant effect in the limit of small heat fluxes and large mass velocities. Nucleation at the wall is the dominant mechanism in the limit of high heat fluxes and small mass velocities. These two regimes can be joined smoothly into a correlation of the Churchill–Usagi type [14], in which $n = 3$:

$$h = (h_{\text{c}}^n + h_{\text{b}}^n)^{1/n} \tag{3}$$

This correlation is based on measurements performed on 13 000 fluids in vertical and horizontal tubes [11–13]. The forced convection coefficient is referenced to the liquid-only case (h_{LO}),

$$\frac{h_c}{h_{LO}} = F = \left\{ \left[(1-x)^{1.5} + 1.9x^{0.6}(1-x)^{0.01} \left(\frac{\rho_L}{\rho_V} \right)^{0.35} \right]^{-2.2} + \left\{ \frac{h_{LO}}{h_{VO}} x^{0.01} \left[1 + 8(1-x)^{0.7} \left(\frac{\rho_L}{\rho_V} \right)^{0.67} \right] \right\}^{-2} \right\}^{-0.5} \tag{4}$$

The heat transfer coefficient decreases drastically after the boiling crisis point, and, if the tube is heated with uniform heat flux, the wall temperature increases considerably. In order to avoid this situation, the outlet quality (x) is limited to the 0.6–0.7 range, such that the second term of Eq. (4) becomes negligible:

$$\frac{h_c}{h_{LO}} = F = \left[(1-x)^{1.5} + 1.9x^{0.6}(1-x)^{0.01} \left(\frac{\rho_L}{\rho_V} \right)^{0.35} \right]^{1.1} \tag{5}$$

For turbulent forced convection in the liquid-only regime, which is a valid model in many practical situations, we rely on the Dittus–Boelter correlation

$$h_{LO} = 0.023 \frac{k_L}{D} \left(\frac{4\dot{m}}{\pi D \eta_L} \right)^{0.8} P_{rL}^{0.4} \tag{6}$$

The heat transfer coefficient in the nucleate boiling limit is estimated with reference to, or as a departure from, the heat transfer coefficient for pool boiling (h_{NB}):

$$\frac{h_b}{h_{NB}} = S = \left(\frac{q''}{q''_0} \right)^n \left(\frac{D}{D_0} \right)^m \left(\frac{R_a}{R_{a0}} \right)^{0.133} S_p S_M S_x \tag{7}$$

When the tubes are horizontal, as in the present application, the parameters for Eq. (7) are [11]:

$$M = 0.56, \quad m = -0.5, \quad S_p = p_r^{0.35}(1 + 17.6p_r^3) \tag{8}$$

$$S_M = M^{0.27},$$

$$S_x(x) = \begin{cases} 1 + 0.35x, & q'' \leqslant 50\,000\ \mathrm{W/m^2} \\ 1, & q'' > 50\,000\ \mathrm{W/m^2} \end{cases} \tag{9}$$

For the calculation of the pool boiling heat transfer coefficient we used the procedure described in Ref. [12, Section Hbb]. If the heat flux is below the value for the onset of nucleate boiling, h_b is zero.

A good evaporator is one where the walls are wetted everywhere by saturated liquid. Such an evaporator is said to be flooded. In a flooded evaporator the recirculation ratio is larger than one, where the recirculation ratio is the number of passes that the stream must make through the evaporator until the evaporation is complete. If the vapor quality of the stream is zero at the inlet, the first law for the control volume drawn around the refrigerant requires

$$\dot{Q} = \dot{m} x_{out} \Delta h_{LV} \tag{10}$$

The recirculation ratio is

$$n = \frac{1}{x_{out}} = \frac{\dot{m} \Delta h_{LV}}{\dot{Q}} \tag{11}$$

where $\dot{Q}$ is the thermal power. When $\dot{Q}$ and the saturation temperature are specified, Eqs. (5)–(7) and (11) show that h_c and h_b depend on n in the following manner:

$$h_c \sim n^{0.8} \tag{12}$$

$$h_b \sim S_x = 1 + 0.35 \frac{x_{out}}{2} = 1 + \frac{0.175}{n} \tag{13}$$

As a qualitative approximation, we superimpose the h_c and h_b effects and obtain

$$h \sim n^{0.8} + 1 + \frac{0.75}{n} \tag{14}$$

which suggests that a maximum h can be found. The more accurate calculation takes into account the fact that in this superposition the h_c and h_b terms are modulated by the factors F and S respectively. Extensive measurements show that the heat transfer rate increases considerably as the recirculation ratio increases from 1 to approximately 3 [15]. Further increases in the recirculation ratio do not lead to significant increases in heat transfer rate, although the pressure drop increases dramatically. In sum, the recirculation ratio must be set in the range 2–5 [15].

We now return to the search for the optimal tube wall temperature, and perform the optimization at constant recirculation ratio, i.e., constant mass flow rate. If we fix $(H/W)_{opt} = 0.83$ and vary the tube diameter (or $D/A^{1/2}$), we obtain the curve with negative slope shown in Fig. 7. When D increases, the temperature difference $T_{peak} - T_w$ decreases because the tube approaches the corner of the elemental cross-section. At the same time, the convective component of the heat transfer coefficient decreases as $h_c \sim D^{-1.8}$, in accordance with Eq. (6). The wall heat flux decreases as $q''_w \sim D^{-1}$. Eq. (7) shows that $h_b \sim (q''_w)^{0.56} \sim D^{-0.56}$, which means that the temperature difference $(T_w - T_b)$ increases with D, while

$$T_w - T_b \sim \frac{1}{D} \frac{1}{D^{-1.8} + D^{-0.56}} \tag{15}$$

This function has a positive slope for practical values of D. We performed the minimization of $(T_{peak} - T_b)$ for the practical case of a skating rink cooled by ammonia refrigerant, at an evaporation temperature $T_b = -20$ °C and recirculation ratio $n = 5$. The results for $(T_{peak} - T_b)$, $(T_w - T_b)$ and $(T_{peak} - T_w)$ are plotted in Fig. 7, where θ_b and θ_{peak} are the dimensionless temperature differences

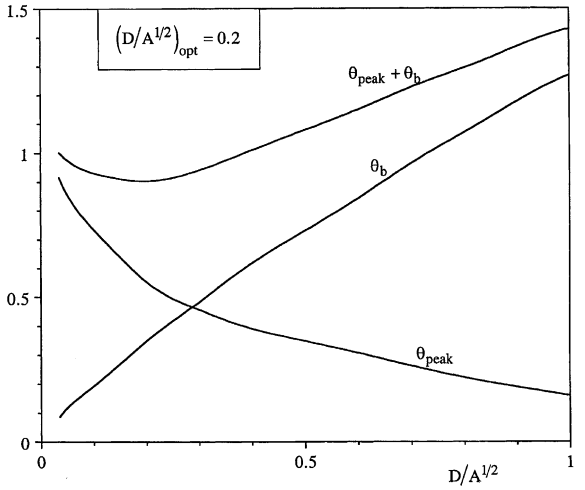

Fig. 7. The selection of the tube diameter by minimizing of the overall temperature difference in the tube cross-section.

$$\theta_b = \frac{T_w - T_b}{(q''/k)(HW)^{1/2}} \tag{16}$$

$$\theta_{peak} = \frac{T_{peak} - T_w}{(q''/k)(HW)^{1/2}} \tag{17}$$

The optimal tube diameter for minimum $(T_w - T_b)$ is $(D/A^{1/2})_{opt} = 0.2$.

In summary, the ratios $(D/A^{1/2})_{opt}$ and $(H/W)_{opt}$ represent the optimal cross-sectional shape of the elemental volume. If the size of the elemental cross-section is fixed, the performance level is the highest when the overall temperature difference $(T_{peak} - T_b)$ is minimum.

5. Optimal shape in the horizontal plane

The next step in the optimization of geometry is the shape of the elemental volume in the horizontal plane: the ratio L/W (Fig. 8). The horizontal area is fixed,

$$A_1 = LW, \quad \text{constant} \tag{18}$$

The objective is to minimize the overall temperature difference $(T_{peak} - T_{b2})$, where T_{b2} is the refrigerant temperature at the outlet port, i.e., the lowest temperature in the elemental volume. When L is large and D small, the high pressure drop experienced by the evaporating fluid will induce a large temperature drop $T_{b1} - T_{b2}$. In this limit W is small, and $(T_{peak} - T_{b1}) \ll (T_{b1} - T_{b2})$. In the opposite extreme (short L), the longitudinal temperature drop $(T_{b1} - T_{b2})$ is small, and the transversal temperature difference $(T_{peak} - T_{b1})$ is large because of two effects: long conduction path, and small heat transfer coefficient inside the tube.

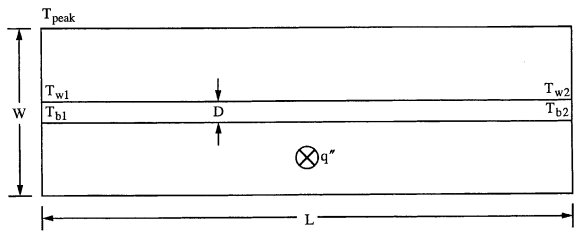

Fig. 8. The elemental volume, viewed from above.

The analysis begins with Eq. (16) and the optimized elemental cross-section, $H/W = 0.83$ and $D/A^{1/2} = 0.2$, which yield

$$\frac{W}{D} = 5.55 = \frac{A_1}{LD} \tag{19}$$

The Clapeyron relation expresses the longitudinal temperature drop in proportion to the pressure drop,

$$\frac{dT}{dp} = \frac{T(v_V - v_L)}{\Delta h_{LV}} \tag{20}$$

The longitudinal pressure gradient is given by [16]

$$\frac{dp}{d\xi} = \left(\frac{dp}{d\xi}\right)_{LO} \Phi_{LO} \quad (0 < \xi < L) \tag{21}$$

where ξ is the longitudinal position, $(dp/d\xi)_{LO}$ is the liquid-only pressure gradient

$$\left(\frac{dp}{dL}\right)_{LO} = -0.079 \frac{32}{\pi^2 \rho_L} \left(\frac{\pi \eta_L}{4}\right)^{0.25} \frac{\dot{m}^{1.75}}{D^{4.75}} \tag{22}$$

and Φ_{LO} is a two-phase flow multiplier

$$\Phi_{LO} = \left(1 + \frac{20}{X_{tt}} + \frac{1}{X_{tt}^2}\right)^{1/2} \tag{23}$$

In these equations η_L and ρ_L are the liquid viscosity and density, and X_{tt} is the Lockhart–Martinelli parameter

$$X_{tt}^2 = \left(\frac{1-x}{x}\right)^{1.8} \frac{\rho_V}{\rho_L} \left(\frac{\eta_L}{\eta_V}\right)^{0.2} \tag{24}$$

Eq. (20) yields

$$\frac{dT}{d\xi} = \frac{dT}{dp}\frac{dp}{d\xi} = -Tc_1 \Phi_{LO} \frac{1}{D^{4.75}} \tag{25}$$

where

$$c_1 = \frac{v_V - v_L}{\Delta h_{LV}} \left[0.079 \frac{32}{\pi^2 \rho_L} \left(\frac{\pi \eta_L}{4}\right)^{0.25}\right] \dot{m}^{1.75} \tag{26}$$

Assuming that the variation in saturation temperature $(T_{b1} - T_{b2})$ is small, we evaluate the thermophysical properties of both phases at an average temperature so that Eq. (25) becomes

$$\frac{dT}{T} = -c_1 \Phi_{LO} D^{-4.75} d\xi \tag{27}$$

In this expression Φ_{LO} is a function of longitudinal position (ξ), and so is the quality,

$$x = \left(\frac{q''\pi D}{\dot{m}\Delta h_{LV}}\right)\xi \tag{28}$$

By integrating Eq. (26) we arrive at the longitudinal temperature drop,

$$\frac{T_{b1}-T_{b2}}{T_{b1}} = 1-\exp\left[-\frac{c_1}{D^{-4.75}}\int_0^{5.55A_1/D}\Phi_{LO}(\xi)\,d\xi\right] = f(D) \tag{29}$$

The numerical optimization reported in Fig. 9 was performed for the same skating rink as in Section 4, for which the assumed thermophysical properties are $\Delta h_{LV} = 1.329\times10^6$ J/kg, $Pr_L = 1.8$, $\rho_V = 1.6$ kg/m^3, $\rho_L = 665$ kg/m^3, $\eta_V = 2.21\times10^{-4}$ Pa s, $\eta_L = 8.5\times10^{-6}$ Pa s, $k_L = 0.56$ W/mK and $c_{pL} = 4560$ J/kg K. The optimization consisted of minimizing the sum $\theta_1+\theta_b$, where θ_1 represents the dimensionless temperature change experienced by the refrigerant, from the inlet (T_{b1}) to the outlet (T_{b2}),

$$\theta_1 = \frac{T_{b1}-T_{b2}}{(q''/k)(HW)^{1/2}} \tag{30}$$

The optimal geometry in the horizontal plane is characterized by

$$\left(\frac{L}{D}\right)_{opt} = 320, \quad \left(\frac{L}{W}\right)_{opt} = 58 \tag{31}$$

Fig. 9 also shows the effect of the drop in saturation temperature (θ_1), which is due to the pressure drop. For small tube lengths the pressure drop is small, and the induced drop in saturation temperature (θ_1) is not significant relative to the overall temperature difference across the elemental volume. The influence of pressure drop becomes important starting with a certain length (L/D). The optimal length of the elemental volume is slightly superior to the value at which the influence of pressure drop can be observed.

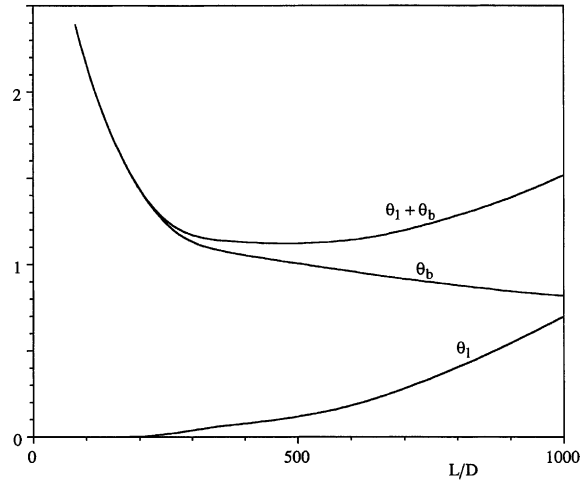

Fig. 9. The selection of the length of the elemental volume by minimizing the overall temperature difference along it.

6. First construct

A larger surface can be covered by arranging in parallel a number (n_1) of optimized elemental volumes, as shown in Fig. 10. In order to equilibrate the flow network, it is a common practice for skating rinks to use orifices or balancing valves that compensate the difference in pressure drop along the headers. In general, only the distribution header is provided with balancing orifices. The collecting header is designed as a low-pressure chamber. However, in the present approach we modeled both headers as a succession of T-shaped fittings connected with tube segments. In order to determine the optimal design of this structure, we searched for the diameters of the distributing and collecting headers (D_{d1}, D_{c1}) by minimizing the pressure drop and the amount of material used in the headers. We also used the notation

$$a_{d1} = \left(\frac{D}{D_{d1}}\right)^2, \quad a_{c1} = \left(\frac{D}{D_{c1}}\right)^2 \tag{32}$$

where D is the diameter of the elemental tubes. The local pressure drops introduced by the kth dividing T in the turbulent flow regime ($Re > 10^4$) are given by [17]:

$$(\Delta p_{k,ab})_d = \tfrac{1}{2}\rho(U_k)_d^2[K_{ab}(k,a_{d1})]_d \tag{33}$$

$$[K_{ab}(k,a_{d1})]_d = 0.03\left(1-\frac{1}{k}\right)^2 + 0.35\frac{1}{k} - 0.1\frac{1}{k}\left(1-\frac{1}{k}\right) \tag{34}$$

$$(\Delta p_{k,ac})_d = \tfrac{1}{2}\rho(U_k)_d^2[K_{ac}(k,a_{d1})]_d \tag{35}$$

$$[K_{ac}(k,a_{d1})]_d = 0.95\left(1-\frac{1}{k}\right)^2 + \frac{1}{k^2}\left(1+\frac{0.4-0.1a_{d1}}{a_{d1}}\right) + 0.4\frac{1}{k}\left(1-\frac{1}{k}\right)\frac{1+a_{d1}}{a_{d1}} \tag{36}$$

Because in the collecting header the refrigerant is in two-phase flow, the large differences between vapor and liquid properties (viscosity, density, velocity) produce significant increases in the local pressure drop. As is shown in Ref. [18], for local resistances for fittings with two-phase flow the pressure drop may be computed based on liquid-only pressure drop and a two-phase flow multiplier (Ψ_{LO}):

$$\Psi_{LO} = 1 + Cx_{out}\frac{v_V - v_L}{v_L}, \quad K_{TP} = K_{LO}\psi_{LO} \tag{37}$$

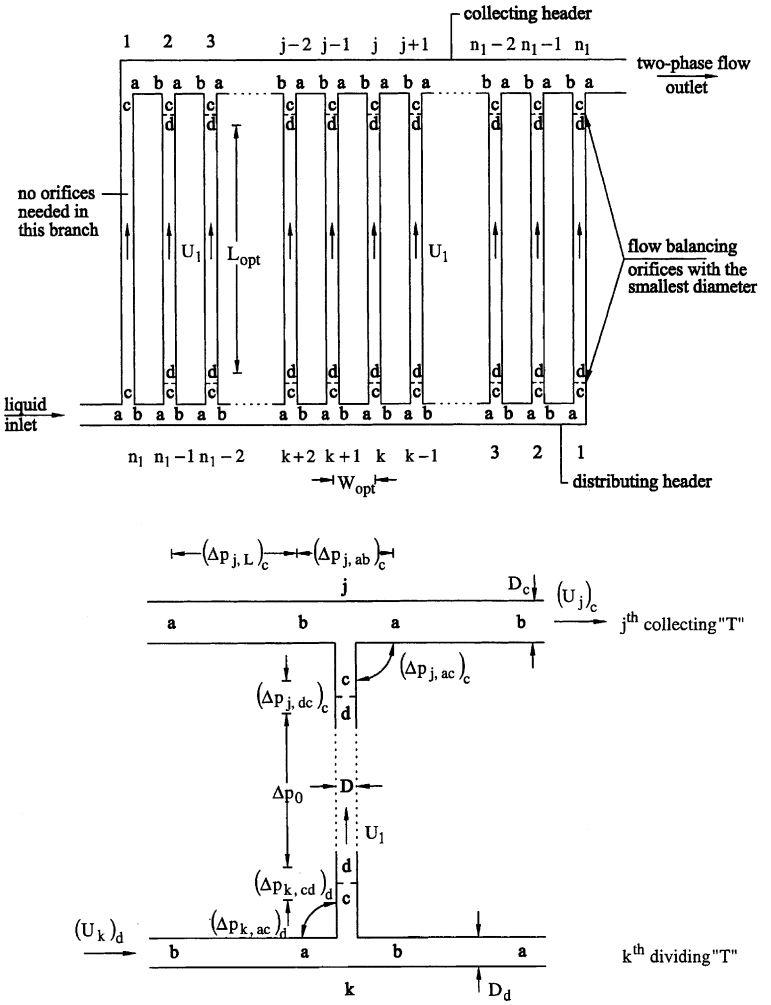

Fig. 10. The construction of the headers as an assemblies of T-shaped fittings linked with tube segments.

where $C = 1.6$ for T fittings, and $C = 0.8$ for orifices. The local pressure drops introduced by the jth collecting T in the turbulent regime ($Re > 10^4$) are [17]:

$$(\Delta p_{j,\mathrm{ab}})_c = \tfrac{1}{2}\rho (U_j)_c^2 [K_{\mathrm{ab}}(j, a_{c1})]_c \Psi_{\mathrm{LO}} \tag{38}$$

$$[K_{\mathrm{ab}}(j, a_{c1})]_c = 0.03\left(1 - \frac{1}{j}\right)^2 + \frac{1}{j^2}[0.62 + 0.38(1 - a_{c1})] + (2 - a_{c1})\left(1 - \frac{1}{j}\right)\frac{1}{j} \tag{39}$$

$$(\Delta p_{j,\mathrm{ac}})_c = \tfrac{1}{2}\rho (U_j)_c^2 [K_{\mathrm{ac}}(j, a_{c1})]_d \Psi_{\mathrm{LO}} \tag{40}$$

$$[K_{\mathrm{ac}}(j, a_{c1})]_d = -0.92\left(1 - \frac{1}{j^2}\right) - \frac{1}{j^2}\left[-1.2 + 0.8\left(1 - \frac{1}{a_{c1}^2}\right)\right] + (2 - a_{c1})\left(1 - \frac{1}{j}\right)\frac{1}{j} \tag{41}$$

In the distributing header, the pressure drop between the liquid inlet and any point labeled "c" in Fig. 10 is maximum at the node (n_1) situated near the inlet. No supplementary local resistance (orifice resistance "dc") is needed for the n_1th elemental tube. The orifice diameter decreases from tube $(n_1 - 1)$ to tube 1.

A similar pattern is present in the collecting header. The largest pressure drop between a point of type "c" and the two-phase flow outlet corresponds to the first tube, where no supplementary orifice resistance "dc" is needed. The orifice diameter decreases starting with the second tube. These features allow us to derive an expression for the pressure drop across the first construct, without having to specify the orifice diameters:

$$\Delta p_1 = \Delta p_0 + (\Delta p_{n_1,\mathrm{ac}})_d + (\Delta p_{1,\mathrm{ac}})_c + \sum_{j=1}^{n_1-1}(\Delta p_{j,\mathrm{L}}) + \sum_{j=2}^{n_1}(\Delta p_{j,\mathrm{ab}})_c \tag{42}$$

The amount of header material used for a given floor area, which must be minimized, is

$$A_1 = \frac{\pi(D_{d1} + D_{c1})(n_1 - 1)W_{opt}}{n_1 W_{opt} L_{opt}} = \frac{\pi(n_1 - 1)}{n_1 (L/D)_{opt}} \left(a_{d1}^{-0.5} + a_{c1}^{-0.5}\right) \quad (43)$$

Assuming that in the first construct the headers are embedded together with the elemental tubes in the same concrete layer, a header diameter larger than ($D/A^{1/2} > 0.8$) weakens the mechanical structure (cf. Section 3). From this observation follow two additional constraints:

$$a_{d1} \geqslant \tfrac{1}{16}, \quad a_{c1} \geqslant \tfrac{1}{16} \quad (44)$$

The first-construct design can be optimized in two ways. One way is to fix the area A_1, minimize the pressure drop, and determine a_{d1} and a_{c1}. The alternative is to fix the pressure drop and minimize A_1. In either case, the pressure drop is bounded from above by a ceiling value (Δp_l) for which the operation of the refrigeration plant is still economical. In the numerical optimization we used the dimensionless constraint

$$\Delta\tilde{p}_l = \frac{\Delta p_l}{\frac{1}{2}\rho U_l^2} = 300 \quad (45)$$

where U_l is the liquid-only velocity in each elemental tube. All the pressure drop components in Eq. (42) may be expressed in dimensionless form by using $\frac{1}{2}\rho U_l^2$ as reference,

$$(\Delta\tilde{p}_{n_1,ac})_d = (n_1 a_{d1})^2 [K_{ac}(n_1, a_{d1})]_d \quad (46)$$

$$(\Delta\tilde{p}_{1,ac})_c = a_{c1}^2 [K_{ac}(1, a_{c1})]_c \Psi_{LO} \quad (47)$$

$$\sum_{j=1}^{n_1-1} (\Delta\tilde{p}_{j,L})_c = f_l \left(\frac{W}{D}\right)_{opt} a_{c1}^{2.375} \sum_{j=1}^{n_1-1} (j^{1.75}) \Phi_{LO}; \quad f_l = 0.079 \left(\frac{U_l D}{\nu}\right)^{-0.25} \quad (48)$$

$$\sum_{j=2}^{n_1} (\Delta\tilde{p}_{j,ab})_c = a_{c1}^2 \sum \left\{ j^2 [K_{ab}(j, a_{c1})]_c \right\} \Psi_{LO} \quad (49)$$

where f_l is the friction coefficient for turbulent flow in the elemental tubes [17]. To summarize, the optimization statement is

$$\min \left\{ A_1(a_{d1}, a_{c1});\ \Delta\tilde{p}_l = 300;\ a_{d1} \geqslant \tfrac{1}{16};\ a_{c1} \geqslant \tfrac{1}{16} \right\} \quad (50)$$

The numerical results are presented in Fig. 11. When n_1 increases, the optimal headers diameters also increase.

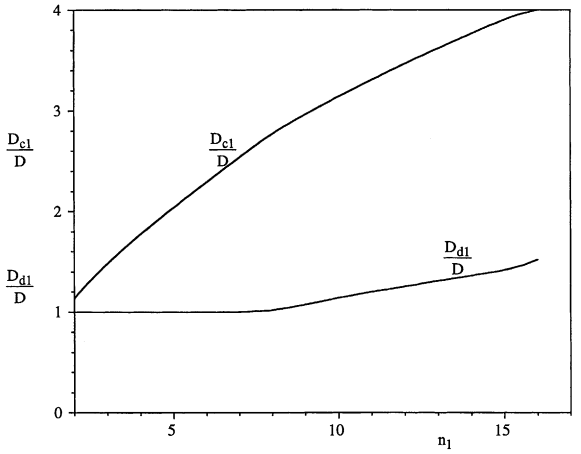

Fig. 11. Optimal header diameters for the first construct as a function of number of elements.

As can be seen in Fig. 11, at $n_1 = 16$ the diameter of the collecting header reaches the maximal value allowed by the constraints (44), that is $D_{c1}/D = 4$. Beyond this stage, the first construct cannot grow because the headers diameters become so large that they cannot be embedded in the concrete layer.

The results of the optimization (50) are the header diameters, a_{d1} and a_{c1}. These values permit the computation of the local pressure drop coefficients for orifices (and, from this, the orifices diameters) from the pressure drop balances on the headers:

$$(\Delta p_{n_1,ab})_d = (\Delta p_{k,cd})_d + (\Delta p_{k,ac})_d + \sum_{i=k}^{n_1-1} (\Delta p_{i,L})_d + \sum_{i=k+1}^{n_1} (\Delta p_{i,ab})_d; \quad (51)$$

$$(K_{k,cd})_d = \frac{(\Delta p_{k,cd})_d}{\frac{1}{2}\rho U_l^2}$$

$$(\Delta p_{j,ac})_c + (\Delta p_{j,dc})_c = \sum_{i=2}^{j} (\Delta p_{i,ab})_c + \sum_{i=1}^{j-1} (\Delta p_{i,L})_c + (\Delta p_{1,ac})_c; \quad (52)$$

$$(K_{j,dc})_c = \frac{(\Delta p_{j,dc})_c}{\frac{1}{2}\rho U_l^2 \Psi_{LO}}$$

In order to obtain the best structures, for constructs of higher order we increased the degree of freedom of the design by abandoning constraint (44): the headers of second constructs can be installed in a plane below the concrete layer.

7. Optimal growth

The second construct consists of a number (n_2) of first constructs. Each first construct contains $n_1 = 16$ elemental volumes: this is the maximal number of elements forming a first construct that can be embedded in the concrete layer (for $n_1 > 16$ the headers weaken the mechanical structure of the concrete layer, or do not fit in its thickness). Constructs of higher order can be made by assembling constructs of lower order so that the total number of elemental volumes used is given by the product $n = n_1 n_2 \cdots n_k$. The objective is to determine the best topology of the tree-shaped network. Using the method of mathematical induction, the following equations for pressure drop and the relative amount of material for headers of a construct of any order can be derived:

$$\begin{aligned}\Delta\tilde{p}_k = \Delta\tilde{p}_{k-1} &+ \left[\prod_{i=1}^{k}(n_i a_{\mathrm{d}i})\right]^2 [K_{\mathrm{ac}}(n_k, a_{\mathrm{d}k})]_{\mathrm{d}} \\ &+ \left[\left(\prod_{i=1}^{k-1} n_1\right)\left(\prod_{i=1}^{k} a_{\mathrm{c}i}\right)\right]^2 \Psi_{\mathrm{LO}} \\ &+ \left(\prod_{i=1}^{k-1} n_k\right)^{1.75}\left(\prod_{i=1}^{k} a_{\mathrm{c}k}\right)^{2.375}\sum_{i=1}^{k-1}(i^{1.75}) f_k \phi_{\mathrm{LO}} \\ &+ \left(\prod_{i=1}^{k} a_{\mathrm{c}i}\right)^2 \sum_{j=2}^{k}\left\{j^2 [K_{\mathrm{ab}}(j, a_{\mathrm{c}k})]_{\mathrm{c}}\right\}\Psi_{\mathrm{LO}} \end{aligned} \tag{53}$$

$$\begin{aligned} f_{2k} &= f_1\left(\prod_{i=1}^{2k} n_{2i}\right)\left(\frac{L}{D}\right)_{\mathrm{opt}}; \\ f_{2k+1} &= f_1(n_1 - 1)\left(\prod_{i=1}^{2k+1} n_{2i+1}\right)\left(\frac{W}{D}\right)_{\mathrm{opt}} \end{aligned} \tag{54}$$

$$a_{\mathrm{d}i} = \left(\frac{D_{\mathrm{d}i}}{D_{\mathrm{d},i-1}}\right)^2; \quad a_{\mathrm{c}i} = \left(\frac{D_{\mathrm{c}i}}{D_{\mathrm{c},i+1}}\right)^2; \quad i = 2, \ldots, n \tag{55}$$

$$\begin{aligned} A_{2k} = A_{2k-1} &+ \frac{\pi}{\left(\prod_{i=1}^{2k-1} n_{2i-1}\right)\left(\frac{W}{D}\right)_{\mathrm{opt}}}\frac{\prod_{i=1}^{2k}(n_{2i}-1)}{\prod_{i=1}^{2k} n_{2i}} \\ &\times \left[\left(\prod_{i=1}^{2k} a_{\mathrm{d}i}\right)^{-0.5} + \left(\prod_{i=1}^{2k} a_{\mathrm{c}i}\right)^{-0.5}\right] \end{aligned} \tag{56}$$

$$\begin{aligned} A_{2k-1} = A_{2k-2} &+ \frac{\pi}{\left(\prod_{i=1}^{2k-2} n_{2i}\right)\left(\frac{L}{D}\right)_{\mathrm{opt}}}\frac{\prod_{i=1}^{2k-1}(n_{2i-1}-1)}{\prod_{i=1}^{2k} n_{2i} - 1} \\ &\times \left[\left(\prod_{i=1}^{2k-1} a_{\mathrm{d}i}\right)^{-0.5} + \left(\prod_{i=1}^{2k-1} a_{\mathrm{c}i}\right)^{-0.5}\right] \end{aligned} \tag{57}$$

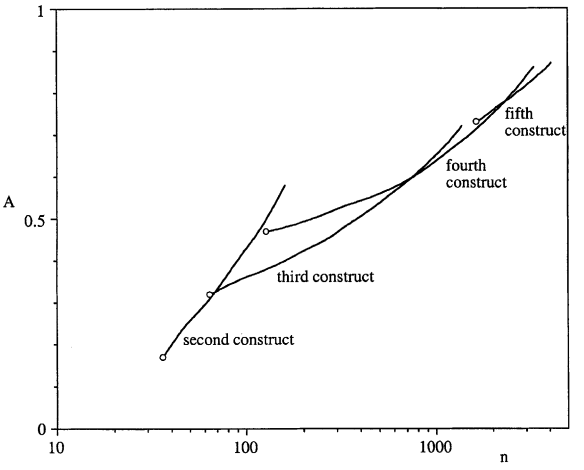

Fig. 12. The amount of headers material relative to the useful surface A, as a function of the number of elements, at fixed pressure drop.

The optimization problem statement for a structure of the kth order is

$$\begin{aligned} &\min\left\{A_k(a_{\mathrm{d}1}, a_{\mathrm{d}2}, \ldots, a_{\mathrm{d}k}, a_{\mathrm{c}1}, a_{\mathrm{c}2}, \ldots, a_{\mathrm{c}k});\right. \\ &\left. a_{\mathrm{d}1} \geqslant \tfrac{1}{16};\ a_{\mathrm{c}1} \geqslant \tfrac{1}{16};\ \Delta\tilde{p}_k = 300\right\} \end{aligned} \tag{58}$$

Fig. 12 was generated as a constructal sequence, by growing the structure up to a construct of the fifth order. The ordinate shows the relative amount of header material defined by Eqs. (56) or (57). The total number of elements (n) is plotted on the abscissa. For example, when the total number of elemental volumes is between 32 and 80, the second construct performs best because it requires the least material relative to other constructs having the same number of elements (i.e. the same total surface serviced). We checked every possible combination of constructs of the second order ($n = n_1 n_2$) and reached the conclusion that the best are those of type $(16 \times k)$ where $k = 2, \ldots, 5$.

We proceeded similarly for constructs of higher order. Only the best configurations are compared in Fig. 12. When $n = 64$, the relative amount of material for the third construct $(16 \times 2 \times 2)$ is slightly higher than for a second order construct (16×4). Starting with $n = 96$, the third constructs perform better because less material is needed to build headers for a structure with $(16 \times 2 \times 3)$ than for one with (16×6). Fourth-order constructs become best starting with $n = 832$. Two constructs of type $(16 \times 2 \times 13)$ can be built with less material than one construct of type $(16 \times 2 \times 26)$ for the same pressure drop. Fifth-order constructs are recommended when $n > 2560$, when a structure of type $(16 \times 2 \times 2 \times 2 \times 20)$ can be built with less material than one of type $(16 \times 2 \times 40 \times 2)$.

After an initially rapid growth of the relative amount of material, the slope of the curve in Fig. 12 (the relative amount of material for headers A, versus the total number of elemental volume n) decreases. At the same time, the number of elements of the optimal construct increases. If, on the other hand, the amount of material for tubes cannot exceed a specified limit, the growth of the dendritic structure must end with a construct of a certain order of complexity.

8. Concluding remarks

In this paper we outlined the optimal design of a tree-shaped network with an evaporating (two-phase) refrigerant, for cooling a surface exposed to uniform heat flux. The design proceeds according to the constructal method, by starting with the simplest (smallest, fixed size) elemental volume, and continuing toward larger assemblies.

The shape of the elemental volume was optimized in three steps. First, the optimal cross-sectional aspect ratio is $(H/W)_{\text{opt}} = 0.83$. This shape is independent of other factors. The second optimization step yielded the best tube diameter. This was achieved by minimizing together the conduction resistance between the corner of the element cross-section and the tube wall, plus the convective resistance between the tube wall and the evaporating refrigerant. Because of the non-linearity of the problem, this step was executed numerically for a specific application (a skating rink). It was found that $(D/A^{1/2})_{\text{opt}} = 0.2$, and that the recirculation ratio must be chosen in the range 2–5. The third optimization of the elemental volume was performed in the horizontal plane, by fixing the elemental area and optimizing its shape. The result was $(L/W)_{\text{opt}} = 58$.

In the second part of the paper, we showed that in order to cover a large area with optimized elemental volumes, the elements must be supplied with refrigerant that flows through a tree-shaped network. The tree was designed for minimum amount of header material and fixed pressure drop. The diameters of the distributing and collecting headers resulted from the optimization. The first construct consisted of n_1 parallel elemental volumes. The headers of the first construct and the elemental tubes were embedded in the concrete layer. By limiting the header diameter to a maximal value that does not weaken the mechanical strength of concrete, we found that n_1 cannot exceed 16.

The headers for constructs of higher order are installed under the concrete layer. This offers considerable freedom in optimizing subsequent stages of the design, because the diameters of such headers are not constrained by mechanical strength considerations. For example, the second construct consists of n_2 first constructs, with 16 elements in each first construct. We showed that the pressure drop along the headers of the second construct dominates the pressure drop along the first-construct header, because $(L/D)_{\text{opt}} > (W/D)_{\text{opt}}$. This means that $n_2 < n_1$, which agrees with earlier features of constructal tree sequences [1,19]. At every step in the growth of the tree structure, the number of elements in the longitudinal (L) direction is smaller than the number of elements in the transversal (W) direction (see Fig. 4). The growth of the network is achieved in alternating fashion: growth in the W direction, growth in the L direction, growth in the W direction, etc. Constructs of various levels of complexity compete: the selected structure is the one that minimizes the amount of header material at fixed pressure drop. The topology of the structure depends on the optimized shape of the elemental volume [$(L/D)_{\text{opt}}$ and $(W/D)_{\text{opt}}$], which is relatively insensitive to operating conditions. It may be influenced, however, by the refrigerant type because of the thermophysical properties, which vary from refrigerant to refrigerant.

The overall conclusion of this work is that it is possible and advantageous to optimize the architecture of tree networks with two-phase flow. The optimized architecture is generated in the pursuit of maximum global performance subject to global constraints. The method and results presented in this paper document the strong connection between flow architecture (geometry) and global performance. Geometry endows the system with the ability to achieve high performance under constraints. This conclusion has important consequences for manufacturers, especially for those in the field of applications cited in Section 1 [4–8]. Accordingly, they can design and manufacture their networks in a modular fashion, the main element being a first construct having a fixed/predetermined number (n_1) of pipes. Additional applications are found in civil engineering [20], for example, the distribution of hot or chilled water over a territory [21,22].

For the special case considered in the figures the skating rink—we conclude that the designer may contemplate performing maintenance work under the rink. This is a very convenient solution, especially when the basement is a parking lot, because it makes it easier to set up the network and headers described above. Analyzed on a case-by-case basis, the optimized tree-shaped network may be preferable to the generally used structure (or registers) of the pipes.

Acknowledgements

Prof. Bejan's work was supported by the National Science Foundation. Prof. Zamfirescu acknowledges the support received from the National Council of Research in Universities, Romania, Grant CNCSiS 95/1999.

References

[1] A. Bejan, Shape and Structure, from Engineering to Nature, Cambridge University Press, Cambridge, UK, 2000.

[2] A. Bejan, M.R. Errera, Convective trees of fluid channels for volumetric cooling, Int. J. Heat Mass Transfer 43 (2000) 3105–3118.

[3] A. Bejan, Dendritic constructal heat exchanger with small-scale crossflows and larger-scales counterlows, Int. J. Heat Mass Transfer 45 (2002) 4607–4620.

[4] D.V. Pence, Improved thermal efficiency and temperature uniformity using fractal-like branching channel networks, in: G.P. Celata, V.P. Carey, M. Groll, I. Tanasawa, G. Zummo (Eds.), Heat Transfer and Transport Phenomena, Begell House, New York, 2000, pp. 142–148.

[5] ASHRAE HVAC Applications Handbook, ASHRAE Press, Atlanta, GA, 1999.

[6] S.P. Rottmayer, W.A. Beckman, J.W. Mitchell, Simulation of a single vertical U-tube ground heat exchanger in an infinite medium, ASHRAE Trans. 103 (1997) 1–9.

[7] C.H.M. Machielsen, Solar powered refrigeration by means of ammonia/water absorption cycles, in: Proc. Workshop on Recent Advances in Solar Energy Technology, Istanbul Technical University & Marmara Research Centre, 1996, pp. 115–127.

[8] K.H. Dress, C.E. Braun, Modeling of area-constrained ice storage tanks, HVAC & R Res. J. 1 (1995) 143–159.

[9] Partial Differential Equation Toolbox User's Guide, Mathworks, Natick, MA, 1997.

[10] C. Zamfirescu, F. Chiriac, Complements of Convection Heat Transfer, Conspress, Bucharest, 2000.

[11] D. Steiner, J. Taborek, Flow boiling heat transfer in vertical tubes correlated as asymptotic model, Heat Transfer Eng. 13 (1992) 43–69.

[12] VDI Wärme Atlas, Verein Deutche Ingenieure, Düsseldorf, 1994.

[13] D. Steiner, M. Ozawa, Flow boiling heat transfer in horizontal and vertical tubes, in: J. Taborek, G. Hewitt, N. Afgan (Eds.), Heat Exchangers—Theory and Practice, Hemisphere, New York, 1983.

[14] S.W. Churchill, R. Usagi, A standardized procedure for the production of correlations in the form of a common empirical equation, Ind. Eng. Chem. Fund. 13 (1974) 39–46.

[15] J. Van Male, E.A. Cosijn, Cooler output as a function of recirculation number of refrigerant recirculation ratio, in: Proc. XIIth Congress of Refrigeration, vol. 2, Madrid, 1967, pp. 945–950.

[16] D. Chisholm, A theoretical basis for the Lockhart–Martinelli correlation for two-phase flow, Int. J. Heat Mass Transfer 10 (1967) 1767–1778.

[17] J. Shetz, A. Fuhs, Handbook of Fluid Mechanics and Fluid Machinery, vol. 3, Wiley, New York, 1996.

[18] P. Griffith, Two-phase flow, in: W.M. Rohsenow, J.P. Hartnett, E.N. Ganic (Eds.), Handbook of Heat Transfer Fundamentals, second ed., McGraw-Hill, New York, 1985.

[19] A. Bejan, Constructal-theory network of conducting paths for cooling a heat generating volume, Int. J. Heat Mass Transfer 40 (1997) 799–816, published on 1 November 1996.

[20] A. Bejan, S. Lorente, Thermodynamic optimization of flow geometry in mechanical and civil engineering, J. Non-Equilib. Thermodyn. 26 (2001) 305–354.

[21] S. Lorente, W. Wechsatol, A. Bejan, Tree-shaped flow structures designed by minimizing path lengths, Int. J. Heat Mass Transfer 45 (2002) 3299–3312.

[22] W. Wechsatol, S. Lorente, A. Bejan, Optimal tree-shaped networks for fluid flow in a disc-shaped body, Int. J. Heat Mass Transfer 45 (2002) 4911–4924.